Journal of Computational and Applied Mathematics 234 (2010) 58–72

Contents lists available at ScienceDirect

Journal of Computational and Applied Mathematics

journal homepage: www.elsevier.com/locate/cam

A simple finite volume method for the shallow water equations

Fayssal Benkhaldoun [a,*], Mohammed Seaïd [b]

[a] LAGA, Université Paris 13, 99 Av J.B. Clement, 93430 Villetaneuse, France

[b] School of Engineering and Computing Sciences, University of Durham, Durham DH1 3LE, UK

ARTICLE INFO

Article history:
Received 28 July 2009
Received in revised form 23 November 2009

Keywords:
Shallow water equations
Finite volume scheme
Method of characteristics
Dam-break problems

ABSTRACT

We present a new finite volume method for the numerical solution of shallow water equations for either flat or non-flat topography. The method is simple, accurate and avoids the solution of Riemann problems during the time integration process. The proposed approach consists of a predictor stage and a corrector stage. The predictor stage uses the method of characteristics to reconstruct the numerical fluxes, whereas the corrector stage recovers the conservation equations. The proposed finite volume method is well balanced, conservative, non-oscillatory and suitable for shallow water equations for which Riemann problems are difficult to solve. The proposed finite volume method is verified against several benchmark tests and shows good agreement with analytical solutions.

1. Introduction

During the last decades there has been an enormous amount of activity related to the construction of approximate solutions for the shallow water equation written in conservative form as

$$\partial_t \begin{pmatrix} h \\ hu \end{pmatrix} + \partial_x \begin{pmatrix} hu \\ hu^2 + \frac{1}{2}gh^2 \end{pmatrix} = \begin{pmatrix} 0 \\ -gh\partial_x Z \end{pmatrix}, \tag{1.1}$$

where $Z(x)$ is the function characterizing the bottom topography, $h(t, x)$ is the height of the water above the bottom, g is the acceleration due to gravity and $u(t, x)$ is the flow velocity. Eq. (1.1) has been widely used to model water flows, flood waves, dam-break problems, and has been studied in a number of books and papers; compare [1–5] among others. Computing their numerical solutions is not trivial due to nonlinearity, the presence of the convective term and the coupling of the equations through the source term. In many applications of (1.1), the convective terms are distinctly more important than the source terms; particularly when certain non-dimensional parameters reach high values (e.g. the Froude number), these convective terms are a source of computational difficulties and oscillations. It is well known that the solutions of Eq. (1.1) present steep fronts and even shock discontinuities, which need to be resolved accurately in applications and often cause severe numerical difficulties [6,2].

Many numerical methods are available in the literature to solve the shallow water equations. One of the most popular techniques is the well-known Roe scheme [7] originally designed for hyperbolic systems without accounting for source terms. In [8], the authors modified the Roe scheme [7] to solve the shallow water equations with source terms in which the idea of balancing the gradient flux with the source term is formulated. This method has been improved in [9] for general channel flows. However, for practical applications, this method may become computationally demanding due to its treatment of the source terms. In the context of well-balanced methods, we mention the work [10] developed to analyze

* Corresponding author. Tel.: +33 1 49403615; fax: +33 1 49403568.
E-mail address: fayssal@math.univ-paris13.fr (F. Benkhaldoun).

0377-0427/$ – see front matter © 2009 Elsevier B.V. All rights reserved.
doi:10.1016/j.cam.2009.12.005

the source term due to cross-section irregularities, and the work in [11] which analyzes the effects of source term in flux difference splitting technique. The authors in [12] have developed exact solutions for the Riemann problem at the interface with a sudden variation in the topography. The main idea in their approach was to define the bottom level such that a sudden variation in the topography occurs at the interface of two cells. A different approach was adopted in quasi-steady wave propagation method in [6]. In this method, an additional Riemann problem in the center of each cell is introduced for balancing the source terms and the flux gradients. An approach based on a local hydrostatic reconstruction has been proposed in [13] for open channel flows with topography. The extension of ENO and WENO schemes to shallow water equations has been studied in [14]. Unfortunately, most ENO and WENO schemes that solves real flows correctly are still very computationally expensive. In the framework of Runge–Kutta discontinuous Galerkin methods, authors in [15] extended the method to a class of hyperbolic system of balance laws with separable source terms. The central idea in this approach is a proper decomposition of the source term allowing well balancing and preserving the genuinely high resolution of the method. However, most of these methods present results with an order of accuracy smaller than the expected in the solutions for unstructured grids, see for example [16]. Besides this fact, it is well known that TVD schemes have their order of accuracy reduced to first order in the presence of shocks due to the effects of limiters. On the other hand, numerical methods based on kinetic reconstructions have been studied in [17], but the complexity of these methods is relevant.

In current work we propose a new family of numerical schemes that incorporate the techniques from method of characteristics into the reconstruction of numerical fluxes. Our main goal is to present a class of numerical methods that are simple, easy to implement, and accurately solves the shallow water equations without relying on a Riemann solver. This goal is reached by integrating twice the shallow water system (1.1) in time and space. In the first integration, Eq. (1.1) is integrated over an Eulerian time–space control volume. We term this step by corrector stage applied to the conservation equations. In the second integration, the shallow water equations are rewritten in a non-conservative form and integrated along the characteristics defined by the water velocity. This step is called predictor stage and used to calculate the numerical fluxes required in the corrector stage. Our method can be treated as a conservative modified method of characteristics for shallow water equations or as a Riemann solver-free finite volume method for shallow water equations. To approximate the characteristic curves an iterative process is used and numerical fluxes are computed by using interpolation procedures. The discretization of flux gradients and source terms are well balanced and the method satisfies the exact C-property. The proposed scheme has the ability to handle calculations of slowly varying flows as well as rapidly varying flows over continuous and discontinuities bottom beds. We should mention that another advantage in using the method of characteristic is that no boundary conditions are needed for the numerical fluxes at the predictor stage. These features are demonstrated using several benchmark problems for shallow water flows. Results presented in this paper show high resolution of the proposed finite volume characteristics method and confirm its capability to provide accurate and efficient simulations for shallow water flows including complex topography.

In this paper, first the finite volume characteristics method is formulated in Section 2. Thereafter, an analysis of stability and convergence is presented in Section 3. Section 4 is devoted to the application of our method to the shallow water equations. After numerical results and examples are presented in Section 5, accuracy and efficiency of the finite volume characteristics scheme are discussed. Concluding remarks end the paper in Section 6.

2. The finite volume characteristics method

To formulate the finite volume characteristics (FVC) scheme we first consider a scalar homogeneous equation of a nonlinear conservation law given by

$$\partial_t u + \partial_x f(u) = 0. \tag{2.1}$$

We discretize the space domain in cells $[x_{i-1/2}, x_{i+1/2}]$ with same length Δx for sake of simplicity. We also divide the time interval into subintervals $[t_n, t_{n+1}]$ with uniform size Δt. Here, $t_n = n\Delta t$, $x_{i-1/2} = i\Delta x$ and $x_i = (i + 1/2)\Delta x$ is the center of the control volume. Integrating Eq. (2.1) with respect to time and space over the time–space control domain $[t_n, t_{n+1}] \times [x_{i-1/2}, x_{i+1/2}]$ shown in Fig. 2.1, we obtain the following discrete equation

$$U_i^{n+1} = U_i^n - \frac{\Delta t}{\Delta x}\left(f(U_{i+1/2}^n) - f(U_{i-1/2}^n)\right), \tag{2.2}$$

where U_i^n is the space average of the solution u in the control volume $[x_{i-1/2}, x_{i+1/2}]$ at time t_n i.e.,

$$U_i^n = \frac{1}{\Delta x}\int_{x_{i-1/2}}^{x_{i+1/2}} u(t_n, x)\, \mathrm{d}x,$$

and $f(U_{i\pm1/2}^n)$ are the numerical fluxes at $x = x_{i\pm1/2}$ and time t_n. The spatial discretization of Eq. (2.2) is complete when a numerical construction of the fluxes $f(U_{i\pm1/2}^n)$ is chosen. In general, this construction requires a solution of Riemann problems at the interfaces $x_{i\pm1/2}$. From a computational viewpoint, this procedure is very demanding and may restrict the application of the method for which Riemann solutions are not available.

In the present work, we reconstruct the intermediate states $U_{i\pm1/2}^n$ using the method of characteristics. The fundamental idea of this method is to impose a regular grid at the new time level and to backtrack the flow trajectories to the previous

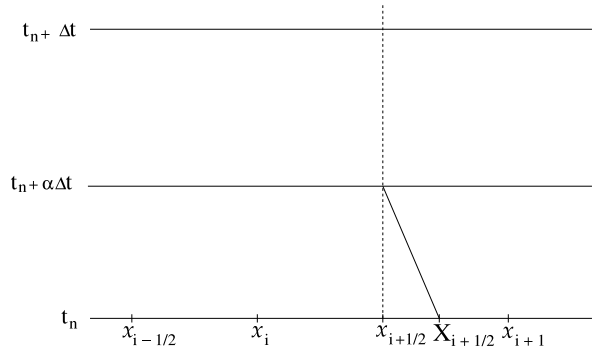

Fig. 2.1. An illustration of control volumes used in the proposed FVC method.

time level. At the old time level, the quantities that are needed are evaluated by interpolation from their known values on a regular grid. Thus, the characteristic curves associated with Eq. (2.1) are solutions of the initial-value problem

$$\begin{aligned} &\frac{\mathrm{d}X_{i+1/2}(\tau)}{\mathrm{d}\tau} = V_{i+1/2}\left(\tau, X_{i+1/2}(\tau)\right), \quad \tau \in [t_n, t_n + \alpha\Delta t], \\ &X_{i+1/2}(t_n + \alpha\Delta t) = x_{i+1/2}, \end{aligned} \tag{2.3}$$

where $V_{i+1/2} = f'(U_{i+1/2})$ and $\alpha \in]0, 1]$ is a parameter to be selected in the sequel. Note that $X_{i+1/2}(\tau)$ is the departure point at time τ of a particle that will arrive at gridpoint $x_{i+1/2}$ in time $t_n + \alpha\Delta t$. The method of characteristics does not follow the flow particles forward in time, as the Lagrangian schemes do, instead it traces backwards the position at time t_n of particles that will reach the points of a fixed mesh at time $t_n + \alpha\Delta t$. By doing so, the method avoids the grid distortion difficulties that the conventional Lagrangian schemes have. The solutions of (2.3) can be expressed as

$$X_{i+1/2}(t_n) = x_{i+1/2} - \int_{t_n}^{t_n+\alpha\Delta t} V_{i+1/2}\left(X_{i+1/2}(\tau)\right)\mathrm{d}\tau. \tag{2.4}$$

For a velocity field explicitly given independent of the solution u, the integral in (2.4) can be determined analytically. In other cases, this integral can be calculated using a second-order extrapolation based on the mid-point rule which is accurate enough to maintain a particle on its curved trajectory. For completeness, the reformulation of the algorithm used to calculate the departure points is detailed in the Appendix. Once the characteristic curves $X_{i+1/2}(t_n)$ are known, the numerical fluxes in (2.2) are reconstructed using

$$U^n_{i+1/2} = u\left(t_n + \alpha\Delta t, x_{i+1/2}\right) = \tilde{U}\left(t_n, X_{i+1/2}(t_n)\right), \tag{2.5}$$

where $\tilde{U}(t_n, X_{i+1/2}(t_n))$ is the solution at the characteristic foot computed by interpolation from the gridpoints of the control volume where the departure point resides i.e.

$$\tilde{U}\left(t_n, X_{i+1/2}(t_n)\right) = \mathcal{P}\left(U\left(t_n, X_{i+1/2}(t_n)\right)\right), \tag{2.6}$$

where $\mathcal{P}$ represents the interpolating polynomial. For instance, a Lagrange-based interpolation polynomials can be formulated as

$$\mathcal{P}\left(U\left(t_n, X_{i+1/2}(t_n)\right)\right) = \sum_k l_k(X_{i+1/2})U^n_k, \tag{2.7}$$

with l_k are the Lagrange basis polynomials given by

$$l_k(x) = \prod_{\substack{q=0 \\ q\neq k}} \frac{x - x_q}{x_k - x_q}.$$

Hence, the proposed FVC scheme can be interpreted as a predictor stage (2.5) where the numerical fluxes $f(U_{i\pm1/2})$ are calculated followed with a corrector stage (2.2) where the conservation property is preserved. Note that other interpolation procedures in (2.6) can also be applied.

It is worth remarking that the introduction of the time parameter α in the predictor stage (2.5) is motivated by the fact that the time step $t_n + \alpha\Delta$ should not be larger than the value t_{n+1} which corresponds to the time required for the fastest wave generated at the interface $x_{i+1/2}$ to leave the cell $[x_i, x_{i+1}]$, compare Fig. 2.1. In our implementation, we have used a global fixed value for α however, a local selection $\alpha^n_{i+1/2}$ is also possible.

3. Analysis of the finite volume characteristics method

In this section we assume a linear interpolating polynomial $\mathcal{P}$ is used in the predictor stage (2.5). Thus, we have the following results:

Lemma 3.1. *Suppose $u_0 \in L^\infty(\mathbb{R})$ with $u_{\min} = \min(u_0)$ and $u_{\max} = \max(u_0)$. Define $\lambda = \sup_{u\in[u_{\min},u_{\max}]} |f'(u)|$, and let Δt satisfy the condition*

$$\frac{1}{2\alpha} \leq \lambda \frac{\Delta t}{\Delta x} \leq \frac{1}{\sqrt{2\alpha}}. \tag{3.1}$$

Then the FVC scheme (2.5) and (2.2) is stable and TVD.

Proof. Applied to the problem (2.1), the corrector stage (2.2) gives

$$U_i^{n+1} = U_i^n - \nu \left(f(U_{i+1/2}^n) - f(U_{i-1/2}^n) \right), \tag{3.2}$$

with $\nu = \frac{\Delta t}{\Delta x}$. The averaged states are given by

$$U_{i+1/2}^n = u\left(t_n + \alpha \Delta t, x_{i+1/2}\right) = u\left(t_n, X_{i+1/2}\right), \tag{3.3}$$

where the characteristic curves are given by

$$X_{i+1/2} = x_{i+1/2} - \alpha \Delta t f'\left(U_{i+1/2}^n\right).$$

Using the linear interpolating polynomial, the solution at the departure points in (3.3) are calculated as

$$\begin{aligned} U_{i+1/2}^n &= U_i^n + \left(X_{i+1/2} - x_i\right) \frac{U_{i+1}^n - U_i^n}{x_{i+1} - x_i}, \\ &= U_i^n + \frac{\frac{\Delta x}{2} - \alpha \Delta t f'\left(U_{i+1/2}^n\right)}{\Delta x} (U_{i+1}^n - U_i^n). \end{aligned} \tag{3.4}$$

Hence, the predictor stage (2.5) becomes

$$U_{i+1/2}^n = \frac{U_i^n + U_{i+1}^n}{2} - \alpha \nu f'(U_{i+1/2}^n) \left(U_{i+1}^n - U_i^n\right). \tag{3.5}$$

Note that we have assumed by construction that the problem (3.5) has a unique solution. There exists $\gamma_i^n \in [U_{i-1/2}^n, U_{i+1/2}^n]$ such that

$$f(U_{i+1/2}^n) - f(U_{i-1/2}^n) = f'(\gamma_i^n) \left(U_{i+1/2}^n - U_{i-1/2}^n\right).$$

Thus, substituting (3.5) in the corrector stage (3.2) we obtain

$$U_i^{n+1} = U_i^n - \nu f'(\gamma_i^n) \left[\left(\frac{1}{2} - \alpha \nu f'(U_{i+1/2}^n) \right) \left(U_{i+1}^n - U_i^n\right) \right] - \nu f'(\gamma_i^n) \left[\left(\frac{1}{2} + \alpha \nu f'(U_{i-1/2}^n) \right) \left(U_i^n - U_{i-1}^n\right) \right],$$

which can be reformulated in a compact form as

$$U_i^{n+1} = U_i^n + C_{i+1/2}^n \Delta U_{i+1/2}^n - D_{i-1/2}^n \Delta U_{i-1/2}^n,$$

where $\Delta U_{i+1/2}^n = U_{i+1}^n - U_i^n$, $C_{i+1/2}^n = \nu f'(\gamma_i^n) \left(\alpha \nu f'(U_{i+1/2}^n) - \frac{1}{2} \right)$ and $D_{i-1/2}^n = f'(\gamma_i^n) \nu \left(\alpha \nu f'(U_{i-1/2}^n) + \frac{1}{2} \right)$.

Under the condition (3.1), it is clear that

$$C_{i+1/2}^n \geq 0, \qquad D_{i-1/2}^n \geq 0, \qquad C_{i+1/2}^n + D_{i-1/2}^n \leq 1. \tag{3.6}$$

Therefore, the characteristic finite volume scheme is L^∞-stable, see Section 3.2 in page 133 from [18]. ■

Lemma 3.2. *Assume a linear interpolating polynomial $\mathcal{P}$ is used in the predictor stage (2.5). The FVC method is second-order accurate scheme if $\alpha = \frac{1}{2}$.*

Proof. By using a linear interpolating polynomial $\mathcal{P}$, the FVC method yields

$$\begin{aligned} U_{i+1/2}^n &= \frac{U_i^n + U_{i+1}^n}{2} - \alpha \frac{\Delta t}{\Delta x} f'\left(U_{i+1/2}^n\right) \left(U_{i+1}^n - U_i^n\right), \\ U_i^{n+1} &= U_i^n - \frac{\Delta t}{\Delta x} \left(f(U_{i+1/2}^n) - f(U_{i-1/2}^n) \right). \end{aligned} \tag{3.7}$$

The FVC method (3.7) can be easily formulated in a compact form as

$$U_i^{n+1} = H\left(U_{i-1}^n, U_i^n, U_{i+1}^n\right). \tag{3.8}$$

Hence, the truncation error associated with (3.8) is defined by

$$u(x, t+\Delta t) - H\left(u(x-\Delta x, t), u(x, t), u(x+\Delta x, t)\right) = -\Delta t^2 \frac{\partial}{\partial x}\left(\beta\left(u, \frac{\Delta t}{\Delta x}\right)\frac{\partial u}{\partial x}\right) + \mathcal{O}\left(\Delta t^3\right), \tag{3.9}$$

where

$$\beta(u, \nu) = \frac{1}{2\nu^2}\sum_{j=-1}^{+1} j^2 \frac{\partial H}{\partial v_j}(u, u, u) - \frac{1}{2}\left(f'(u)\right)^2.$$

The proof of the Lemma 3.2 follows from the Proposition 1.2 in page 103 from [18] which states that if β vanishes in (3.9), then the scheme (3.8) is second-order accurate. Indeed,

$$\frac{\partial H}{\partial U_{i+1}} = -\nu f'\left(U_{i+1/2}^n\right)\frac{\partial U_{i+1/2}^n}{\partial U_{i+1}},$$
$$\frac{\partial H}{\partial U_{i-1}} = \nu f'\left(U_{i-1/2}^n\right)\frac{\partial U_{i-1/2}^n}{\partial U_{i-1}}.$$

Hence,

$$\frac{\partial H}{\partial U_{i+1}}(u, u, u) = -\nu f'(u)\left(\frac{1}{2} - \alpha\nu f'(u)\right),$$
$$\frac{\partial H}{\partial U_{i-1}}(u, u, u) = \nu f'(u)\left(\frac{1}{2} + \alpha\nu f'(u)\right).$$

Thus,

$$\beta = \left(\alpha - \frac{1}{2}\right)\left(f'(u)\right)^2.$$

It is clear that for $\alpha = \frac{1}{2}$, the parameter $\beta = 0$ and this resumes the proof. ■

4. Application to the shallow water equations

The extension of the FVC method for hyperbolic systems of conservation laws can be carried out componentwise provided that the conservative equations can be rewritten in an advective formulation. In general, the advective form of the system under study is built such that the non-conservative variables are transported with the same velocity field. In the current study, to apply the FVC method for the shallow water equation (1.1), we first reformulated the shallow water equations in an advective form as

$$\partial_t\begin{pmatrix} h \\ u \end{pmatrix} + u\partial_x\begin{pmatrix} h \\ u \end{pmatrix} = \begin{pmatrix} -h\partial_x u \\ -g\,\partial_x(h+Z) \end{pmatrix}. \tag{4.1}$$

Then, we calculate the characteristic curves $X_{i+1/2}(\tau)$ associated to (4.1) as

$$\begin{aligned} &\frac{\mathrm{d}X_{i+1/2}(\tau)}{\mathrm{d}\tau} = u\left(\tau, X_{i+1/2}(\tau)\right), \quad \tau \in [t_n, t_n + \alpha\Delta t], \\ &X_{i+1/2}(t_n + \alpha\Delta t) = x_{i+1/2}, \end{aligned} \tag{4.2}$$

where u is the velocity of the water flow. The initial-value problem (4.2) is solved using the algorithm described in the Appendix. The numerical fluxes in the FVC schemes are obtained by integrating the system (4.1) along the characteristics in the time interval $[t_n, t_n + \alpha\Delta t]$. Assume an accurate approximation of the characteristics curves $X_{i+1/2}(t_n)$ is made, the predictor stage in the FVC method applied to the shallow water equations is defined by

$$\begin{aligned} h_{i+1/2}^n &= \tilde{h}_{i+1/2}^n - \alpha\nu\tilde{h}_{i+1/2}^n\left(u_{i+1}^n - u_i^n\right), \\ u_{i+1/2}^n &= \tilde{u}_{i+1/2}^n - \alpha\nu g\left(\left(h^n + Z\right)_{i+1} - \left(h^n + Z\right)_i\right), \end{aligned} \tag{4.3}$$

where $\nu = \frac{\Delta t}{\Delta x}$ and

$$\tilde{h}_{i+1/2}^n = h\left(t_n, X_{i+1/2}(t_n)\right), \qquad \tilde{u}_{i+1/2}^n = u\left(t_n, X_{i+1/2}(t_n)\right),$$

are the solutions at the characteristic foot computed by interpolation from the gridpoints of the control volume where the departure point $X_{i+1/2}(t_n)$ belongs.

Remark 4.1. It should be stressed that another way to calculate the numerical fluxes in the predictor stage is to consider the advection version of the shallow water equations

$$\partial_t \begin{pmatrix} h \\ hu \end{pmatrix} + u\partial_x \begin{pmatrix} h \\ hu \end{pmatrix} = \begin{pmatrix} -h\partial_x u \\ -hu\partial_x u - \dfrac{1}{2}g\partial_x\left(h^2\right) - gh\partial_x Z \end{pmatrix}. \tag{4.4}$$

Hence, the predictor stage becomes

$$\begin{aligned} h^n_{i+1/2} &= \tilde{h}^n_{i+1/2} - \alpha\nu\tilde{h}^n_{i+1/2}\left(u^n_{i+1} - u^n_i\right), \\ q^n_{i+1/2} &= \tilde{q}^n_{i+1/2} - \alpha\nu\tilde{q}^n_{i+1/2}\left(u^n_{i+1} - u^n_i\right) - \frac{1}{2}\alpha\nu g\left(\left(h^2\right)^n_{i+1} - \left(h^2\right)^n_i\right) - \alpha\nu g\tilde{h}^n_{i+1/2}\left(Z_{i+1} - Z_i\right), \end{aligned} \tag{4.5}$$

where $q = hu$ is the water discharge and

$$\tilde{h}^n_{i+1/2} = h\left(t_n, X_{i+1/2}(t_n)\right), \qquad \tilde{q}^n_{i+1/2} = q\left(t_n, X_{i+1/2}(t_n)\right),$$

with the departure points $X_{i+1/2}(t_n)$ are obtained by solving the initial-value problem (4.2). Notice that in both systems (4.1) and (4.4) the variables (h, u) and (h, hu) are transported with the same velocity field. In our simulations, using the system (4.1) or (4.4) in the predictor stage of FVC method produces similar results.

The corrector stage in the FVC method gives

$$\begin{aligned} h^{n+1}_i &= h^n_i - \nu\left(h^n_{i+1/2}u^n_{i+1/2} - h^n_{i-1/2}u^n_{i-1/2}\right), \\ q^{n+1}_i &= q^n_i - \nu\left(\left(hu^2 + \frac{1}{2}gh^2\right)^n_{i+1/2} - \left(hu^2 + \frac{1}{2}gh^2\right)^n_{i-1/2}\right) - \frac{1}{2}\nu g\hat{h}^n_i\left(Z_{i+1} - Z_{i-1}\right), \end{aligned} \tag{4.6}$$

where $q = hu$ is the water discharge. In our FVC method, the reconstruction of the term $\hat{h}^n_i$ in (4.6) is carried out such that the discretization of the source term is well balanced with the discretization of flux gradients using the concept of C-property [8]. Here, a numerical scheme is said to satisfy the C-property for Eq. (1.1) if the condition

$$h^n + Z = C = \text{constant}, \qquad u^n = 0, \tag{4.7}$$

holds for stationary flows at rest. Therefore, the treatment of source terms in (4.6) is reconstructed such that the condition (4.7) is preserved at the discretized level.

Let us assume a stationary flow at rest, $u = 0$ and a linear interpolation procedure is used in the FVC method. Thus, the system (1.1) reduces to

$$\partial_t \begin{pmatrix} h \\ 0 \end{pmatrix} + \partial_x \begin{pmatrix} 0 \\ \dfrac{1}{2}gh^2 \end{pmatrix} = \begin{pmatrix} 0 \\ -gh\partial_x Z \end{pmatrix}. \tag{4.8}$$

Applied to the system (4.8), the predictor stage in (4.3) computes

$$\begin{aligned} h^n_{i+1/2} &= \frac{h^n_i + h^n_{i+1}}{2}, \\ u^n_{i+1/2} &= 0, \end{aligned} \tag{4.9}$$

while the corrector stage in (4.6) updates the solution as

$$\begin{aligned} h^{n+1}_i &= h^n_i, \\ q^{n+1}_i &= q^n_i - \frac{1}{2}\nu g\left(\left(h^n_{i+1/2}\right)^2 - \left(h^n_{i-1/2}\right)^2\right) - \Delta t g\left(h\partial_x Z\right)^n_i. \end{aligned} \tag{4.10}$$

To obtain a stationary solution $h^{n+1}_i = h^n_i$, the sum of discretized flux gradient and source term in (4.10) should be equal to zero i.e.,

$$g\frac{1}{2\Delta x}\left(\left(h^n_{i+1/2}\right)^2 - \left(h^n_{i-1/2}\right)^2\right) = -\left(gh\partial_x Z\right)^n_i. \tag{4.11}$$

Using $h^n_{i+1/2} = \frac{h^n_i + h^n_{i+1}}{2}$, the condition (4.11) is equivalent to

$$g\frac{1}{8\Delta x}\left(h^n_{i+1} + 2h^n_i + h^n_{i-1}\right)\left(h^n_{i+1} - h^n_{i-1}\right) = -\left(gh\partial_x Z\right)^n_i. \tag{4.12}$$

Table 5.1
Error norms for the Burgers problem at time $t = 1$ using different gridpoints.

M	L^∞-error	Order	L^1-error	Order
50	5.7351E−06	–	2.6236E−06	–
100	1.4745E−06	1.9596	6.7452E−07	1.9596
200	3.7387E−07	1.9796	1.7103E−07	1.9796
400	9.4074E−08	1.9907	4.3037E−08	1.9906

Since for stationary solution $h^n_{i+1} - h^n_{i-1} = Z_{i+1} - Z_{i-1}$, Eq. (4.12) becomes

$$(gh\partial_x Z)^n_i = g\frac{h^n_{i+1/2} + h^n_{i-1/2}}{2}\frac{Z^n_{i+1} - Z^n_{i-1}}{2\Delta x}. \tag{4.13}$$

Hence, if the source term $\hat{h}^n_i$ in the corrector stage of (4.6) is discretized as

$$\hat{h}^n_i = \frac{1}{4}\left(h^n_{i+1} + 2h^n_i + h^n_{i-1}\right), \tag{4.14}$$

then the proposed FVC method satisfies the C-property. Notice that this property is achieved by assuming a linear interpolation procedure in the predictor stage of the FVC method. However, a well-balanced discretization of flux gradients and source terms for a quadratic or cubic interpolation procedures can be carried out using similar techniques.

5. Numerical examples

In this section we perform numerical tests with our finite volume characteristics method on the shallow water equations. In all our computations a fixed courant number CFL $= 0.8$ is used while the time step Δt is varied according to the stability condition

$$\Delta t = \mathrm{CFL}\frac{\Delta x}{\max\limits_{k=1,2}\left(\left|\lambda^n_k\right|\right)},$$

where λ_1 and λ_2 are the two eigenvalues of the shallow water equation (1.1). In all results presented in this section the time parameter $\alpha = \frac{1}{2}$ and linear interpolation procedure is used in the predictor stage unless stated. The following test examples are selected:

5.1. Accuracy test problem

We check the accuracy of the proposed FVC method for the Burgers equation

$$\partial_t u + \partial_x\left(\frac{u^2}{2}\right) = 0, \tag{5.1}$$

augmented by the initial condition

$$u(0, x) = x. \tag{5.2}$$

The Burgers problem (5.1)–(5.2) has an exact solution defined as

$$U(t, x) = \frac{x}{1 + t}. \tag{5.3}$$

This example can also serve to test the ability of the FVC method to converge to the correct entropy solution. Recall that the unique entropy solution of (5.1)–(5.2) is smooth up to the critical time $t = 1.5$. Here, we have computed the approximate solution at the pre-shock time $t = 1$ when the solution is still smooth and error norms are presented. We consider the L^∞- and L^1-error norms defined as

$$\max_{1\le i\le M}|u_i - U(x_i)| \quad \text{and} \quad \sum_{i=1}^{M}|u_i - U(x_i)|\,\Delta x, \tag{5.4}$$

respectively. In (5.4), u_i and $U(x_i)$ are respectively, the computed and exact solutions at gridpoint x_i, whereas M stands for the number of gridpoints used in the spatial discretization. The obtained results are listed in Table 5.1 along with their corresponding convergence rates. It reveals that increasing the number of gridpoints in the computational domain results in a decay of both error norms. Our FVC method exhibits good convergence behaviour for this nonlinear scalar problem. As can be seen from the convergence rates presented in Table 5.1, a second-order accuracy is achieved for this test example in terms of the considered error norms.

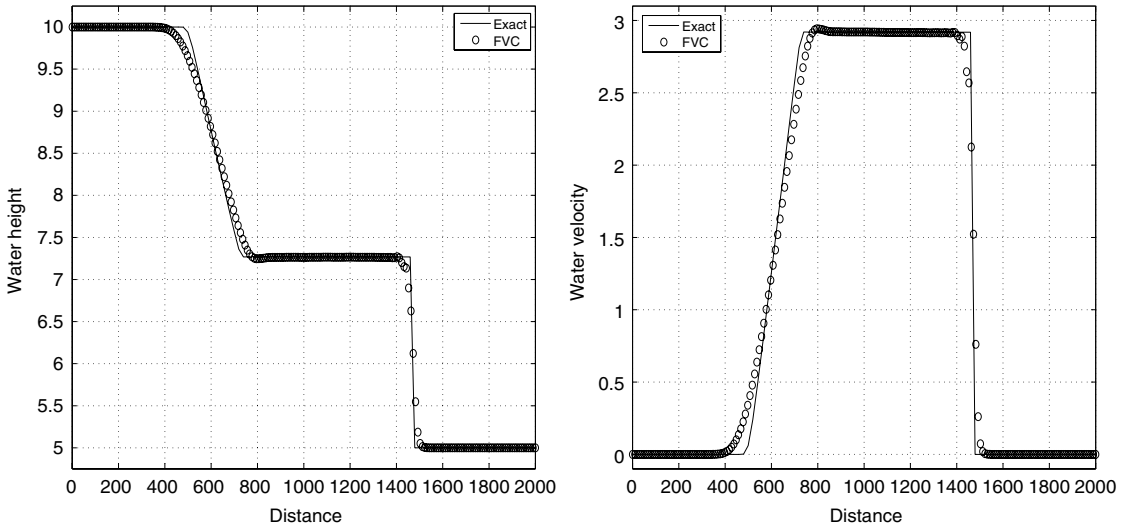

Fig. 5.1. Water height (left plot) and water velocity (right plot) for dam-break on wet bed at $t = 50$ s using $\Delta x = 10$ m, $h_r/h_l = 0.5$.

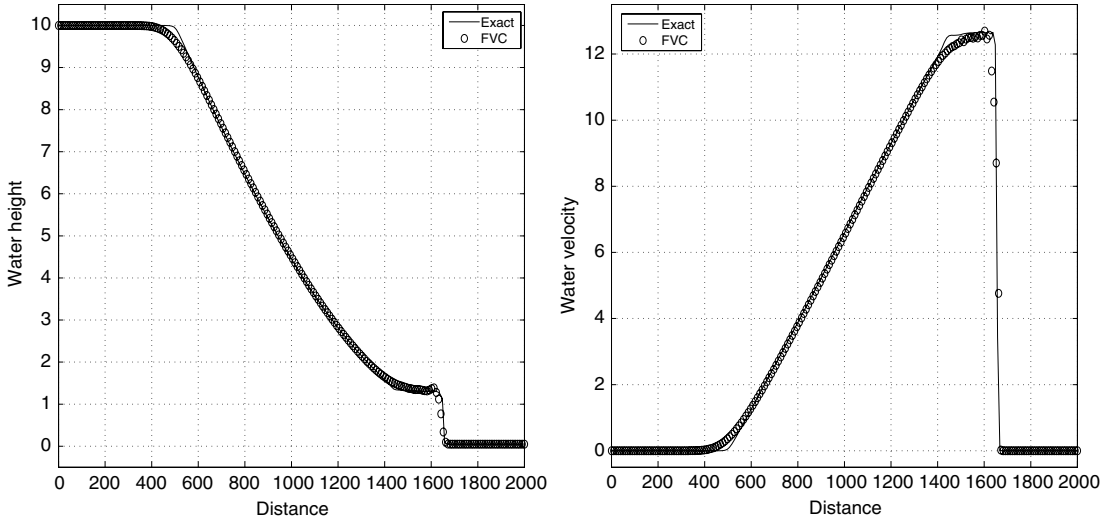

Fig. 5.2. Water height (left plot) and water velocity (right plot) for dam-break on wet bed at $t = 50$ s using $\Delta x = 10$ m, $h_r/h_l = 0.005$.

5.2. Dam-break problem

We consider the dam-break problem in a rectangular channel with flat bottom, $Z(x) = 0$. The channel is of length 2000 m, the space discretization $\Delta x = 10$ m and the initial conditions are given by

$$h(0,x) = \begin{cases} h_l, & \text{if } x \leq 1000 \text{ m}, \\ h_r, & \text{if } x > 1000 \text{ m}, \end{cases} \qquad u(0,x) = 0 \text{ m/s},$$

where $h_l > h_r$ in order to be consistent with the physical phenomenon of a dam-break from the left to the right. At $t = 0$ the dam collapses and the flow problem consists of a shock wave traveling downstream and a rarefaction wave traveling upstream. We start by assuming that in both sides of the dam there are water with corresponding heights $h_l = 10$ m and $h_r = 5$ m (depth ratio $h_r/h_l = 0.5$), for the second test $h_l = 10$ m and $h_r = 0.05$ m (depth ratio $h_r/h_l = 0.005$). Note that the flow structure in the channel is subcritical for depth ratio greater than 0.5, and is supercritical when depth ratio becomes smaller than 0.5. In Figs. 5.1 and 5.2 we plot water height and velocity field at $t = 50$ s for the depth ratio $h_r/h_l = 0.5$ and 0.005, respectively. The FVC scheme captures correctly the discontinuity and the shock without need for very fine mesh. It should be stressed that the performance of our FVC method is very attractive since the computed solutions remain stable and highly accurate without solving Riemann problems or linear systems of algebraic equations.

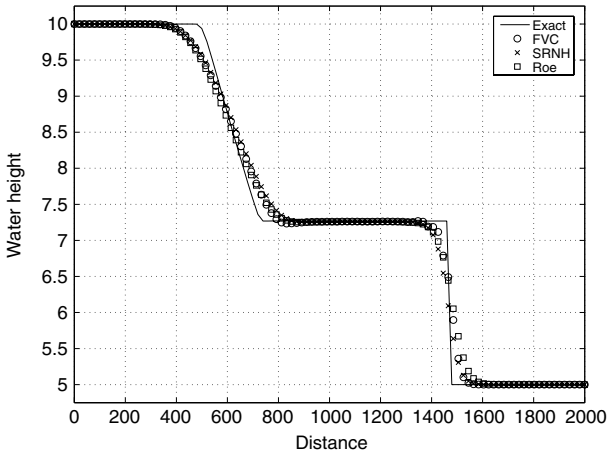

Fig. 5.3. Comparative results for water height in dam-break on wet bed at $t = 50$ s using $\Delta x = 20$ m, $h_r/h_l = 0.5$.

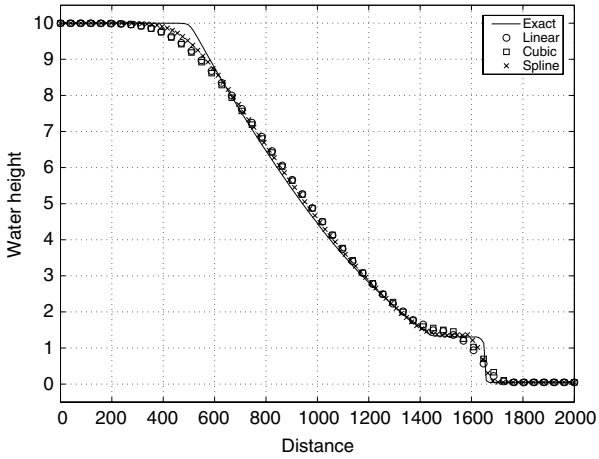

Fig. 5.4. Comparative results for water height in dam-break on wet bed at $t = 50$ s using $\Delta x = 20$ m, $h_r/h_l = 0.005$.

Table 5.2
Computational times in seconds for dam-break on wet bed at $t = 50$ s using $h_r/h_l = 0.005$ and different gridpoints.

Gridpoints	Roe method	SRNH method	FVC method
500	8.746	13.193	1.008
1000	34.780	52.655	2.707
2000	134.152	210.620	15.756
4000	534.124	834.055	61.096
8000	2178.701	3378.303	249.209

To compare the accuracy of our FVC scheme to the Roe scheme originally introduced in [7], we have reproduced the results for the dam-break at subcritical regime (depth ratio $h_r/h_l = 0.5$) using the Roe scheme and the FVC method. We also compare our results to those obtained using the SRNH (Solveur de Riemann Non Homogène) scheme recently proposed and studied in [19]. The computed water heights are displayed in Fig. 5.3 at time $t = 50$ s using a space discretization $\Delta x = 20$ m. For the considered dam-break conditions, the FVC scheme produces numerical results as accurate as those computed using the SRNH and Roe schemes but with a low computational cost, see Table 5.2. The CPU times are measured on a PC with AMD-K6 200 processor running MATLAB codes under Linux 2.2. A simple inspection of Table 5.2 reveals that, for meshes with low number of gridpoints, the measured CPU time is comparable for all considered methods. However, for meshes with large number of gridpoints the FVC method is the most efficient. For instance, for a mesh of 500 gridpoints, the FVC method is about 13 and 9 faster than the SRNH method and Roe scheme, respectively. Note that the SRNH and Roe schemes require a solver for the Riemann problem at each time step to reconstruct the numerical fluxes, which is completely avoided in our FVC scheme.

Next we examine the performance of the FVC scheme using different interpolation procedures in the predictor stage. To this end we illustrate in Fig. 5.4 the water height obtained for the dam-break at supercritical regime (depth ratio

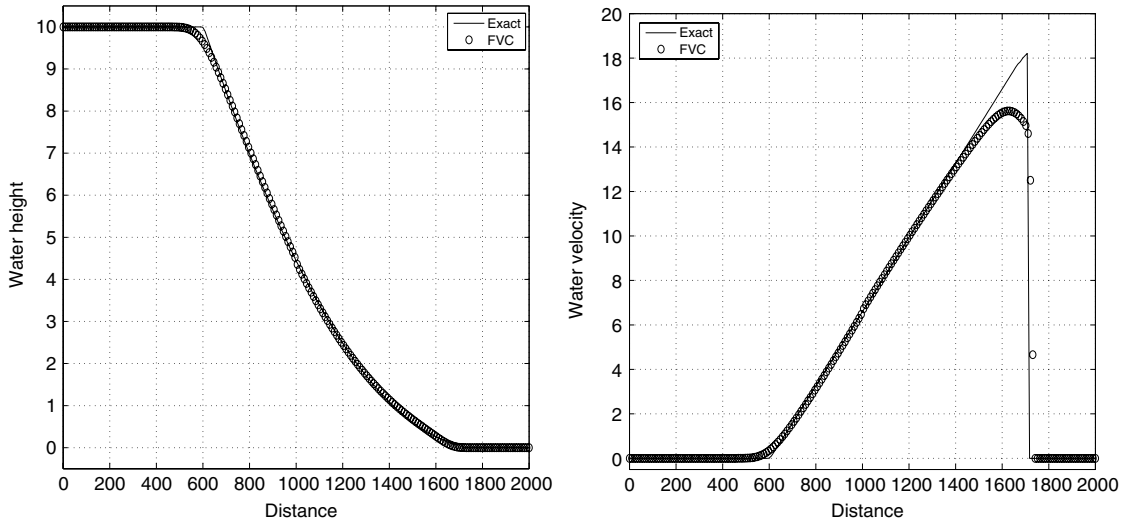

Fig. 5.5. Water height (left plot) and water velocity (right plot) for dam-break on dry bed at $t = 40$ s using $\Delta x = 10$ m, $h_r/h_l = \infty$.

$h_r/h_l = 0.005$) at time $t = 50$ s using three types of interpolation procedures. We have used the linear, cubic and spline interpolations on a coarse spatial discretization with $\Delta x = 20$ m. We observe that the considered interpolation methods produce roughly the same results for this test example. Similar features have been observed for the water velocities. We can also see that the spline interpolation is clearly superior to the other interpolation procedures. In particular, for the shock and rarefaction areas the spline interpolation produces the most accurate results of all the interpolation methods considered.

Our next concern is to ascertain the behaviour of the FVC scheme in presence of dry area. Here, we consider a dry bed in the downstream of the dam, $h_l = 10$ m and $h_r = 0$ m (depth ratio $h_r/h_l = \infty$). This example is more difficult than the previous one because of the singularity that occurs at the transition point of the advancing front. The water height and the velocity flow at $t = 40$ s are depicted in Fig. 5.5. These results are in very close agreement with the exact solution and with small conservation error in velocity variable due to the fact that the interpolation procedure in (4.3) reduces to first-order accuracy in area where the velocity peak is localized. No oscillations or negative values have been observed in the solution. It should be pointed out that our FVC scheme does not require any entropic modifications to treat the dry bed. The analytical reference solutions for these test problems are due to [1].

5.3. Lake at rest flow

In this example we solve the benchmark problem of a lake at rest flow proposed in [8] to test the conservation property of numerical methods for shallow water equations. The lake bed is irregular, so this test example is a good illustration of the significance of the source term treatment for practical applications to natural watercourses. It is expected that the water free-surface remains constant and the water velocity should be zero at all times. We run the FVC method using 100 gridpoints and the obtained results are displayed at time $t = 10\,800$ s. In Fig. 5.6 we present the water free-surface along with the lake bed. We also include in this figure the error in the water free-surface for better insight. As can be seen, the water free-surface remains constant during the simulation times and the proposed FVC method preserves the C-property to the machine precision. It should be stressed that the performance of the FVC method is very attractive since the computed solution remains stable and accurate even when coarse meshes are used without requiring complicated techniques to balance the source terms and flux gradients as those reported in [9,14,10,11,5,13] among others.

5.4. Flow over a hump

To investigate the ability of our FVC method to preserve the correct steady state solutions, we apply the scheme to a series of benchmark test problems for subcritical and transcritical flows. They are widely used to test numerical algorithms for the shallow water equations. In all these test examples the channel length is 25 m and the bottom topography Z is defined as

$$Z(x) = \begin{cases} 0.2 - 0.05(x-10)^2, & \text{if } 8 \le x \le 12, \\ 0, & \text{otherwise.} \end{cases} \tag{5.5}$$

The initial conditions are given by

$$h(0,x) + Z(x) = H \text{ m}, \qquad u(0,x) = 0 \text{ m/s}. \tag{5.6}$$

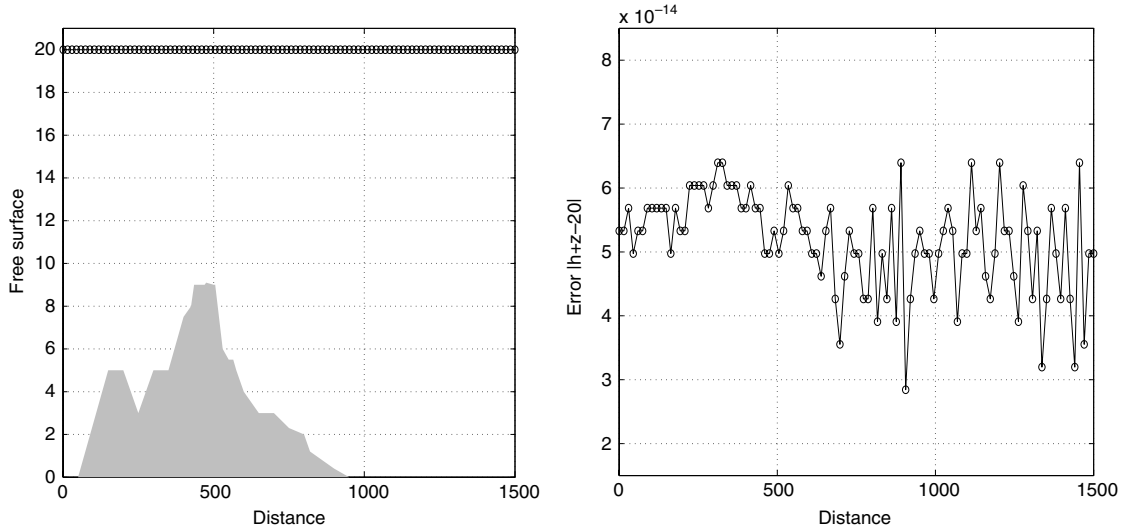

Fig. 5.6. The free-surface for the lake at rest at time $t = 10\,800$ s.

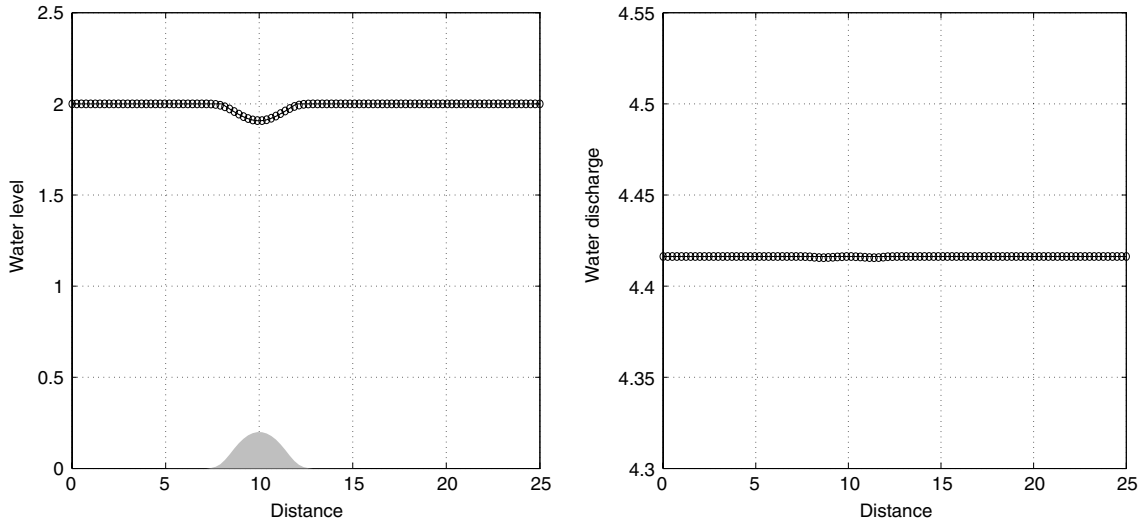

Fig. 5.7. Water height (left plot) and water discharge (right plot) for subcritical flow at $t = 200$ s using 100 gridpoints.

Numerical results are shown for the flow at rest, the subcritical flow, the transcritical flow without shock, and the transcritical flow with shock. All these results are displayed at $t = 200$ s using 100 gridpoints. The analytical solutions are also plotted (by solid lines) within the obtained numerical results.

Subcritical flow: We solve Eqs. (1.1) and (5.5)–(5.6) subject to an upstream boundary condition on the discharge $hu = 4.42$ m^2/s and a downstream condition on the height $H = 2$ m. The obtained results are shown in Fig. 5.7 for the water level and discharge. As can be seen in this figure, the FVC scheme preserves the correct steady flow to almost machine accuracy.

Transcritical flow without shock: In this test case, we solve Eqs. (1.1) and (5.5)–(5.6) using an upstream boundary condition for the discharge $hu = 1.53$ m^2/s and a downstream boundary condition for the water level $H = 0.66$ m only if the flow is subcritical. If the flow is supercritical, no condition is imposed. Fig. 5.8 shows the water level and the discharge plots. Once again, the FVC scheme resolves accurately this test problem with small errors in the discharge plot over the hump area. As mentioned by many authors, the correct capturing of the discharge is more difficult than the water height in these test problems.

Transcritical flow with shock: This test problem is similar to the previous one but with different boundary conditions. Here, a discharge of $hu = 0.18$ m^2/s is imposed as the upstream boundary condition and a water level of $H = 0.33$ m as the downstream boundary condition. The obtained results for this test are displayed in Fig. 5.9. In this figure we have also included the results obtained using a coarse mesh of 100 gridpoints for a better insight. It is evident that, the scheme

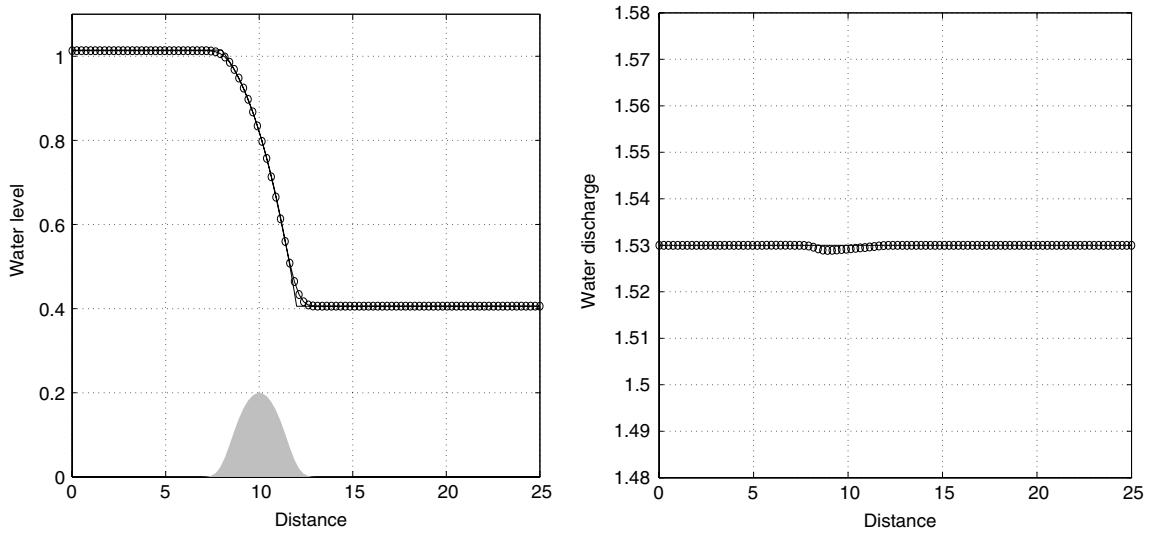

Fig. 5.8. Water height (left plot) and water discharge (right plot) for transcritical flow without shock at $t = 200$ s using 100 gridpoints.

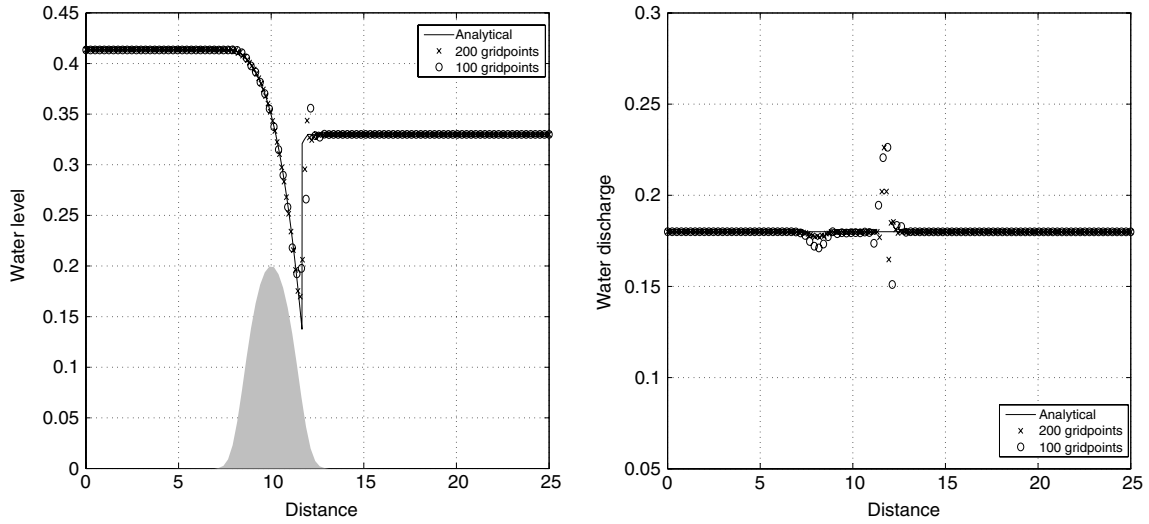

Fig. 5.9. Water height (left plot) and water discharge (right plot) for transcritical flow with shock at $t = 200$ s.

produces small errors in the water discharge on the hump region. The amplitude of these perturbations decreases as the number of gridpoints increases. In comparison with the results reported in [15] for the flow over a hump, the present FVC scheme provides a good accuracy such as the solution of flow discharge. It should be stressed that, due to the use of characteristics method, the proposed FVC scheme may not be suitable for shallow water flows developing strong shocks.

5.5. Drain on a non-flat bottom

This is a challenging numerical test example as it involves the calculation of dry areas in the computational domain. As proposed in [4], the length of the channel is 25 m and the bed profile Z is mathematically defined by (5.5). The initial conditions are

$$h(0, x) + Z(x) = 0.5 \text{ m}, \qquad u(0, x) = 0 \text{ m/s}.$$

Reflective conditions are used on the upstream boundary and the downstream boundary condition is that of a dry bed. The steady state solution of this problem is a flow at rest, in the left part of the hump $h + Z = 0.2$ m, $u = 0$ m/s and dry flow, $h = 0$ m, $u = 0$ m/s in the right of the hump.

We discretize the space domain into 100 uniform gridpoints. In Fig. 5.10 we present the evolution of water depth at several times $t = 10$, $t = 20$, $t = 50$ and $t = 200$ s. The FVC scheme performs very well for this case and gives results

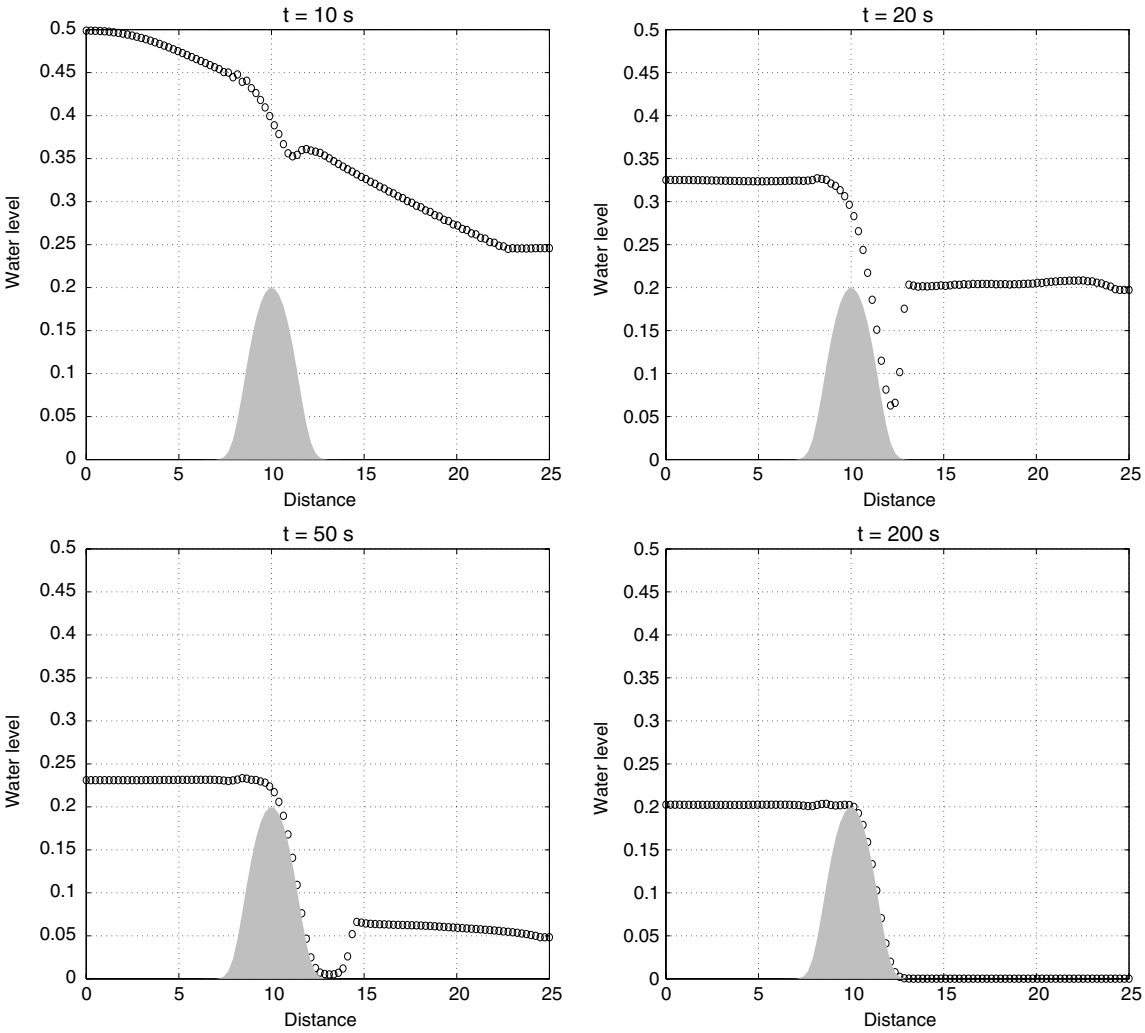

Fig. 5.10. Water height for drain on non-flat bottom at different times.

which converge to the expected steady state solution. These results compare well with those published in [4]. Notice that no modifications have been added to the method to overcome the dry areas in the computational domain. However, to overcome the zero speeds in the FVC method, we perturb these characteristic speeds by 10^{-9} far from zero. The monotonicity of the scheme is preserved and no nonphysical oscillations or extra numerical diffusion have been detected during the computations.

6. Conclusions

A simple and accurate finite volume characteristics method to solve the shallow water equations has been presented. The method combines the attractive attributes of the finite volume discretization and the method of characteristics to yield a procedure for either flat or non-flat topography. The new method has several advantages. First, it can solve steady flows over irregular beds without large numerical errors, thus demonstrating that the proposed scheme achieves perfect numerical balance of the gradient fluxes and the source terms. Second, it can compute the numerical flux corresponding to the real state of water flow without relying on Riemann problem solvers. Third, reasonable accuracy can be obtained easily and no special treatment is needed to maintain a numerical balance, because it is performed automatically in the integrated numerical flux function. Finally, the proposed approach does not require either nonlinear solution or special front tracking techniques. Furthermore, it has strong applicability to various conservative numerical schemes as shown in the numerical results.

The proposed finite volume characteristics method has been tested on systems of shallow water equations at different flow regimes. The obtained results indicate good shock resolution with high accuracy in smooth regions and without any nonphysical oscillations near the shock areas. The convergence to the correct steady state solution has been clearly verified in

flow at rest and drain on non-flat bottom. Although we have restricted our numerical computations to the one-dimensional shallow water problems, the current finite volume characteristics scheme can be straightforwardly extended to shallow water problems in two space dimensions with bottom friction and Coriolis forces. These and further issues are subject of future investigations.

Acknowledgements

This work was partly performed while the second author was a visiting professor at LAGA, Université Paris 13. Financial support provided by LAGA, Université Paris 13 is gratefully acknowledged. The authors also wish to thank the anonymous reviewers for their helpful comments on an earlier draft of the manuscript.

Appendix. Calculation of characteristic curves

To approximate the integral in (2.4), we used a method first proposed in [20] in the context of semi-Lagrangian schemes to integrate the weather prediction equations. Hence, we use $\delta_{i+1/2}$ to denote the displacement between a mesh point on the new level, x_i, and the departure point of the trajectory to this point on the previous time level $X_{i+1/2}(t_n)$, *i.e.*

$$\delta_{i+1/2} = x_{i+1/2} - X_{i+1/2}(t_n).$$

Applying the mid-point rule to approximate the integral in (2.4) yields

$$\delta_{i+1/2} = \alpha \Delta t V_{i+1/2}\left(t_{n+1/2}, X_{i+1/2}(t_{n+\alpha/2})\right). \tag{6.1}$$

Using the second-order extrapolation

$$V_{i+1/2}(t_{n+1/2}, x_{i+1/2}) = \frac{3}{2}V_{i+1/2}(t_n, x_{i+1/2}) - \frac{1}{2}V_{i+1/2}(t_{n-1}, x_{i+1/2}), \tag{6.2}$$

and the second-order approximation

$$X_{i+1/2}(t_{n+1/2}) = x_{i+1/2} - \frac{1}{2}\delta_{i+1/2},$$

we obtain the following implicit formula for $\delta_{i+1/2}$

$$\delta_{i+1/2} = \alpha \Delta t \left[\frac{3}{2}V_{i+1/2}\left(t_n, x_{i+1/2} - \frac{1}{2}\delta_{i+1/2}\right) - \frac{1}{2}V_{i+1/2}\left(t_{n-1}, x_{i+1/2} - \frac{1}{2}\delta_{i+1/2}\right)\right].$$

To compute $\delta_{i+1/2}$ we consider the following successive iteration procedure:

$$\begin{aligned}
\delta^{(0)}_{i+1/2} &= \alpha \Delta t \left[\frac{3}{2}V_{i+1/2}\left(t_n, x_{i+1/2}\right) - \frac{1}{2}V_{i+1/2}\left(t_{n-1}, x_{i+1/2}\right)\right], \\
\delta^{(k)}_{i+1/2} &= \alpha \Delta t \left[\frac{3}{2}V_{i+1/2}\left(t_n, x_{i+1/2}\frac{1}{2}\delta^{(k-1)}_{i+1/2}\right)\right] - \Delta t \left[\frac{1}{2}V_{i+1/2}\left(t_{n-1}, x_{i+1/2} - \frac{1}{2}\delta^{(k-1)}_{i+1/2}\right)\right], \quad k = 1, 2, \ldots.
\end{aligned} \tag{6.3}$$

The iterations (6.3) are terminated when the following criteria

$$\frac{\left\|\delta^{(k)} - \delta^{(k-1)}\right\|}{\left\|\delta^{(k-1)}\right\|} < \varepsilon, \tag{6.4}$$

are fulfilled for the L^∞-norm $\|\cdot\|$ and a given tolerance ε. It is also known [21] that

$$\left\|\delta - \delta^{(k)}\right\| \leq \frac{1}{4}\left\|\delta - \delta^{(k-1)}\right\| \|\partial_u V\| \alpha \Delta t, \quad k = 1, 2, \ldots. \tag{6.5}$$

Hence, a necessary condition for the convergence of iterations (6.3) is that the velocity gradient satisfies

$$\|\partial_u V\| \alpha \Delta t < 1. \tag{6.6}$$

Note that the condition (6.6) is sufficient to guarantee that the characteristics curves do not intersect during a time step of size $\alpha \Delta t$. A schematic representation of the quantities involved in computing the departure points is shown in Fig. 6.1.

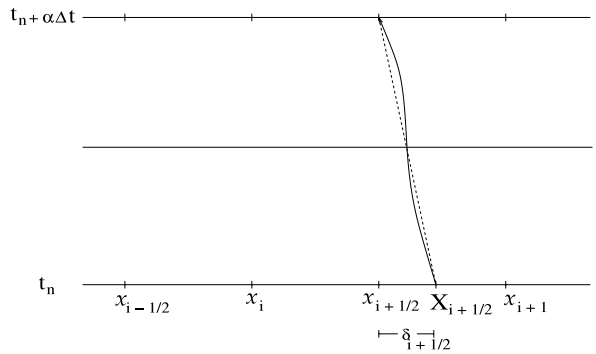

Fig. 6.1. A schematic diagram showing the main quantities used in the calculation of the departure points. The exact trajectory is represented by a solid line and the approximate trajectory with a dashed line.

References

[1] J.J. Stoker, Water Waves, Interscience Publishers, Inc., New York, 1986.
[2] E.F. Toro, Shock-Capturing Methods for Free-Surface Shallow Flows, Wiley and Sons, 2001.
[3] F. Alcrudo, P.G. Navarro, A high resolution Godunov-type scheme in finite volumes for the 2D shallow water equations, Internat. J. Numer. Methods Fluids 16 (1993) 489–505.
[4] T. Gallouët, J.M. Herard, N. Seguin, Some approximate Godunov schemes to compute shallow water equations with topography, Comput. & Fluids 32 (2003) 479–513.
[5] J. LeVeque Randall, Balancing source terms and flux gradients in high-resolution Godunov methods: The quasi-steady wave-propagation algorithm, J. Comput. Phys. 146 (1998) 346–365.
[6] J. LeVeque Randall, Numerical Methods for Conservation Laws, 2nd ed., in: Lectures in Mathematics ETH Zürich, 1992.
[7] P.L. Roe, Approximate Riemann solvers, parameter vectors and difference schemes, J. Comput. Phys. 43 (1981) 357–372.
[8] A. Bermudez, M.E. Vázquez-Cendón, Upwind methods for hyperbolic conservation laws with source terms, Comput. & Fluids 23 (1994) 1049–1071.
[9] M.E. Vázquez, Improved treatment of source terms in upwind schemes for the shallow water equations in channels with irregular geometry, J. Comput. Phys. 148 (1999) 497–526.
[10] P. Garcia-Navarro, M.E. Vazquez-Cendon, On numerical treatment of the source terms in the shallow water equations, Comput. & Fluids 29 (2000) 951–979.
[11] M.E. Hubbard, P. Garcia-Navarro, Flux difference splitting and the balancing of source terms and flux gradients, J. Comput. Phys. 165 (2000) 89–125.
[12] F. Alcrudo, F. Benkhaldoun, Exact solutions to the Riemann problem of the shallow water equations with a bottom step, Comput. & Fluids 30 (2001) 643–671.
[13] E. Audusse, F. Bouchut, M.O. Bristeau, R. Klein, B. Perthame, A fast and stable well-balanced scheme with hydrostatic reconstruction for shallow water flows, SIAM J. Sci. Comput. 25 (2004) 2050–2065.
[14] S. Vukovic, L. Sopta, ENO and WENO schemes with the exact conservation property for one-dimensional shallow-water equations, J. Comput. Phys. 179 (2002) 593–621.
[15] Y. Xing, C. Shu, High order well-balanced finite volume WENO schemes and discontinuous Galerkin methods for a class of hyperbolic systems with source terms, J. Comput. Phys. 214 (2006) 567–598.
[16] R.A. Walters, E. Hanert, J. Pietrzak, D.Y. Le Roux, Comparison of unstructured, staggered grid methods for the shallow water equations, Ocean Model. 28 (2009) 106–117.
[17] M. Seaïd, Non-oscillatory relaxation methods for the shallow water equations in one and two space dimensions, Internat. J. Numer. Methods Fluids 46 (2004) 457–484.
[18] P.A. Raviart, E. Godlewski, Hyperbolic Systems of Conservation Laws, in: Collection Mathematiques et Applications, SMAI, Ellipses Eds, N 3/4, 1990.
[19] S. Sahmim, F. Benkhaldoun, F. Alcrudo, A sign matrix based scheme for quasi-hyperbolic non-homogeneous PDEs with an analysis of the convergence stagnation problem, J. Comput. Phys. 226 (2007) 1753–1783.
[20] C. Temperton, A. Staniforth, An efficient two-time-level semi-Lagrangian semi-implicit integration scheme, Q. J. R. Meteorol. Soc. 113 (1987) 1025–1039.
[21] J. Pudykiewicz, A. Staniforth, Some properties and comparative performance of the semi-Lagrangian method of Robert in the solution of advection–diffusion equation, Atmos.-Ocean 22 (1984) 283–308.